Design Parameters for "Robust" Superoleophobic Surfaces

K. Y. Law,[1*] H. Zhao[1] and K-C Park[2]

[1]Xerox Research Center Webster, Xerox Innovation Group, Webster, NY, USA, (lawkockyee@gmail.com); [2]Department of Mechanical Engineering, Massachusetts Institute of Technology, Cambridge, MA,USA

ABSTRACT

Earlier we reported the fabrication of a model superoleophobic surface comprising ~3 μm diameter pillar arrays (height ~7.8 μm, pitch 6 μm) on silicon wafer via the conventional photolithography and surface fluorosilanation techniques. Results showed that both surface fluorination and the re-entrant structure in the pillar are crucial in achieving superoleophobicity and superhydrophobicity with hexadecane and water contact angles exceeding 150° and sliding angles at ~10°. In this work, we investigate design parameters for the fabrication of a superoleophobic surface that is robust against wetting breakthrough pressure and mechanical abrasion. By studying the effects of pillar height, size and spacing, we show that both static and advancing contact angles remain "super" (>150°) as the pillar size and spacing vary, the receding contact angle, sliding angle and contact angle hysteresis, on the other hand, are found to be sensitive to these structural changes. The receding angle decreases and both sliding angle and hysteresis increase as the solid area fraction increases. Interestingly, surface superoleophobicity remains as the height of the pillar decreases from ~7.8 to 1 μm. Surface Evolver simulation was used to model the location of the contact line as well as the robustness in wetting against external pressure. The abrasion resistance of the pillar array surface was assessed by mechanical modeling and nanoindenter measurement. The design space for fabricating a mechanically robust superoleophobic surface is discussed.

Keywords: Superoleophobicity, surface texturing, design parameters, robustness, breakthrough pressure

1 INTRODUCTION

Printing engines are basically electromechanical devices that put marks of toner and ink on paper. Traditionally, both engine design and print process development are based on optimization of the electromechanical properties. Relatively less attention has been paid to the property of the print surface. As it turns out, contamination of the print surfaces has been an issue all along and the usual countermeasure is to just clean it off. This approach is effective, but adds cost and complexity to the engine design. As our demands on performance, cost and sustainability increase, there is a need for future engine to be smaller, simpler with lower cost. Inspired by the Lotus effect [1], we thought that print surface that can self-clean would radically improve the performance of future engines. Concurrently, we also recognized that surfaces with superhydrophbocity are unlikely to succeed, as most superhydrophobic surfaces are superoleophilic [2] and they will have a high affinity towards organic contaminants in the print engines, such as toner and ink. Thus, surface with superoleophobic property has been our prime target. Earlier, we [3] reported the fabrication of a model superoleophobic surface via photolithography followed by surface fluorination with a fluorosilane. The surface, comprising arrays of 3 μm diameter pillars (6 μm pitch) on silicon wafer, exhibits water and hexadecane contact angles of >150° and sliding angles at ~10°. Systematic investigation revealed that both surface fluorination and surface texturing, particularly the re-entrant structure in the side wall of the pillar, are crucial in achieving the Cassie-Baxter superoleophobic state. On the other hand, pillar arrays with high aspect ratio are known to be weak against mechanical abrasion and transition of the Cassie-Baxter state to the fully wetted Wenzel state is known to occur under high external pressure. Here we study the effect of surface texturing on the wettability of the pillar array surface. The robustness of the surface against wetting and mechanical abrasion is assessed by Surface Evolver simulation [4] and mechanical modeling [5], respectively. The design space for fabricating a mechanically robust superoleophobic surface is discussed.

2 EXPERIMENTAL

All the textured surfaces studied in this work were fabricated on 4" test grade Silicon wafers (Montco Silicon Technologies, Inc.) by the conventional photolithographic technique followed by surface modification with a ~1.5 nm thick fluorosilane layer (FOTS), which was obtained by molecular vapor deposition of tridecafluoro-1,1,2,2-tetrahydrooctyltrichlorosilane onto the bare textured surface in a MVD100 reactor from Applied Mircostructures, Inc. The fluorinated textured surface was heat cured in an oven at ~150°C for ~30 minutes prior to the contact angle measurement. Schematics and details of the procedures have been given elsewhere [3]. Static contact angle and

sliding angle measurements were performed on a goniometer model OCA20 from Dataphysics. The drop size of the test liquid was controlled to be ~5 μL. The advancing/receding contact angles were measured using the sessile drop method by adding/removing liquid to/from the existing droplet at a rate of 0.15 μL/s. The sliding angles were measured using the tilting base unit accessory TBU 90. After dispensing a 10 μL droplet, the stage was tilted about one degree per second to a maximum of 90°. The sliding angle is defined as the angle where the test liquid droplet starts to move.

3 RESULTS AND DISCUSSION

3.1 Effect of Surface Texturing on Surface Properties

Figures 1a-1d show the SEM micrographs of 4 different textured FOTS surfaces comprising 3 μm diameter pillar arrays (height ~7 μm) with center-to-center spacing varying from 4.5 to 6 to 9 to 12 μm on Si wafer. Their surface properties were studied by both static and dynamic contact angle measurements. Photographs of the water and hexadecane sessile drops are given in the insets of Figure 1 which show that all four pillar array surfaces exhibit water and hexadecane contact angles @ ~150°. Figure 2 plots the sliding angles for the water and hexadecane droplets as a function of the solid area fraction of the pillar array surface (solid=1.0). The results indicate that the sliding angle decreases as the solid area fraction decreases. The generally small sliding angle along with the large static contact angle lead us to conclude that these surfaces are all superhydrophobic and superoleophobic at the same time.

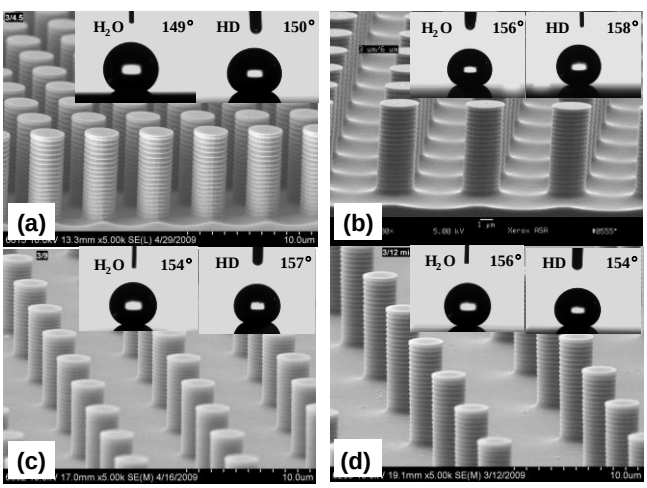

Fig. 1 SEM micrographs of the ~3 μm pillar array FOTS surfaces with (a) 4.5 μm, (b) 6 μm, (c) 9 μm, and (d) 12μm pillar spacing. (Insets: sessile drops of water and hexadecane on the pillar array surfaces)

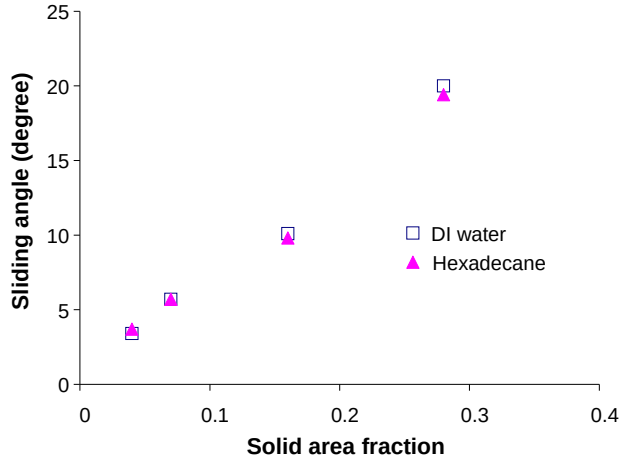

Fig. 2 Plot of sliding angles for the water and hexadecane droplets as a function of solid area fraction.

Figures 3 and 4 plot the advancing & receding contact angle and the hysteresis for the four pillar array FOTS surfaces as a function of solid area fraction for water and hexadecane, respectively.

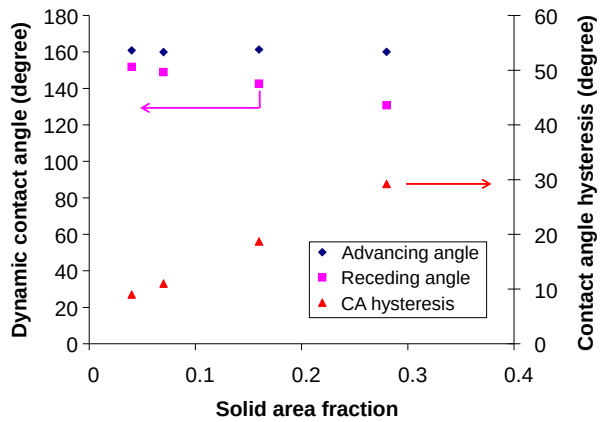

Fig. 3 Plot of advancing & receding water contact angle and hysteresis vs. the solid area fraction.

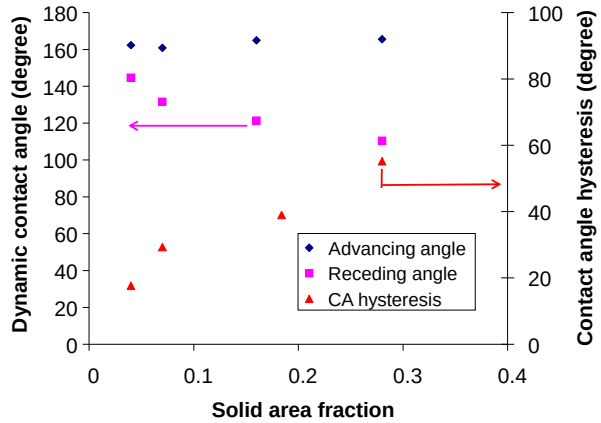

Fig. 4 Plot of advancing & receding hexadecane contact angle and hysteresis vs. the solid area fraction.

The overall results in Figures 1-4 reveal that varying the pillar spacing or the solid area fraction has little effect on the static and advancing contact angle. On the other hand, sliding angle and hysteresis increase and receding angle decreases as the solid area fraction is increasing. The solid area fraction effect is larger for hexadecane, presumably because hexadecane has a lower contact angle on the FOTS surface and its surface tension is lower. A more detailed discussion of the solid area fraction effect on the dynamic contact angle will be given elsewhere [6].

In addition to pillar spacing, we have also studied the effect of pillar diameter [6] and height on the surface properties. The results plotted in Figures 5 and 6 reveal that both static and dynamic water and hexadecane contact angles are insensitive to pillar height down to ~1 μm. We have evidence that both water and hexadecane droplets become less stable at 0.8 μm pillar height, suggesting that water and hexadecane droplets may sag and transition from the Cassie-Baxter state to the Wenzel state due to wetting of the bottom of the pillar surface.

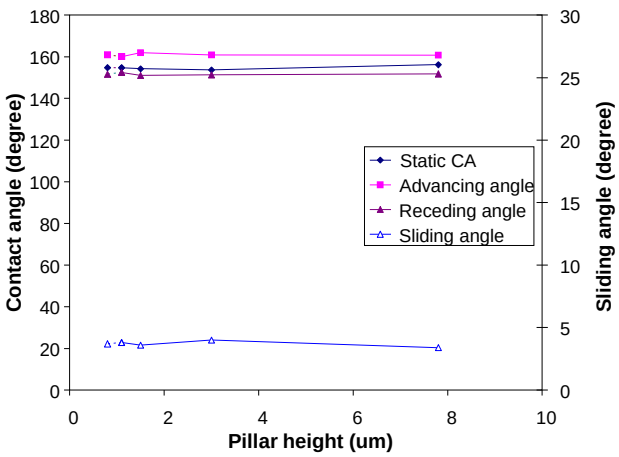

Fig. 5 Plot of static and dynamic water contact angle data for 3 μm pillar array FOTS surface vs. pillar height.

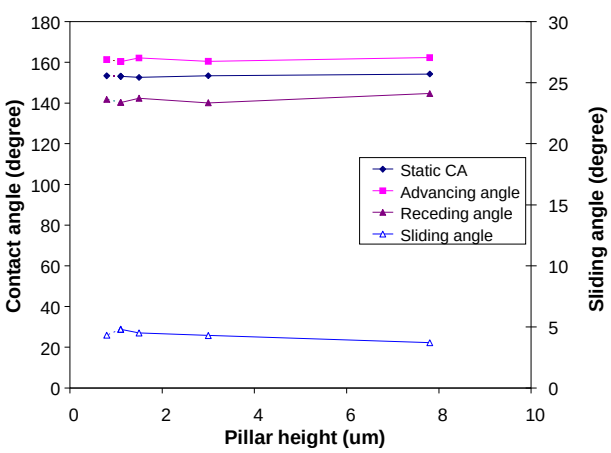

Fig. 6 Plot of static and dynamic hexadecane contact angle data for 3 μm pillar array FOTS surface vs. pillar height.

3.2 Modeling Wetting and Mechanical "Robustness"

Robustness of Wetting Under Pressure. Surface Evolver simulation was used to compute the equilibrium shape of the liquid-vapor interfaces by minimizing various energies of the interfaces under user-specified initial condition and constraints. In the present work, we employ it to (1) simulate the location of the liquid-solid-vapor three phase contact line on the re-entrant structure, (2) depict the sagging curvature of the liquid-vapor interface, and (3) estimate the wetting robustness against pressure. The breakthrough pressure is defined as the threshold that triggers the transition from the Cassie-Baxter state to the Wenzel state. Figure 7 depict the liquid-vapor interface for hexadecane on a 3 μm diameter pillar array (6 μm pitch) FOTS surface. The modeling suggests that droplet of hexadecane pins underneath the re-entrant structure of the pillar array surface. This was validated experimentally where we were able to create a replica of the composite interface using a polyethylene wax mold and studied the morphology of the interface by SEM microscopy.[3]

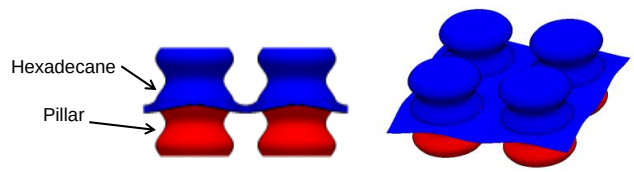

Fig. 7 Equilibrium shapes of sagging liquid-air interface of hexadecane on a superoleophobic pillar array FOTS surface.

Using Surface Evolver simulation, the effect of pillar size, spacing and diameter on the breakthrough pressure of the pillar array FOTS surface was studied and typical result is given in Figure 8.

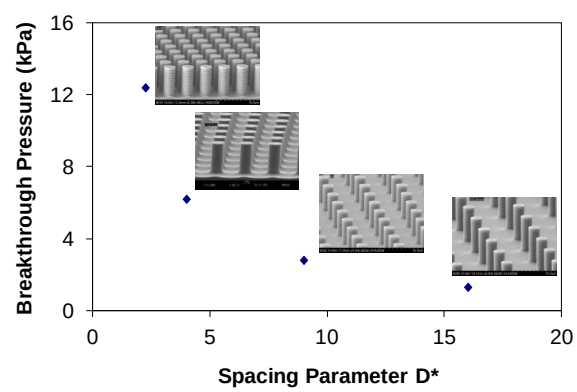

Fig. 8 Plot of breakthrough pressure versus spacing parameter D*.

D* is defined as $(W + D)^2/W^2$, where 2W is the diameter of the pillar and 2D is the separation distance between two pillars. The result suggests that smaller pillar diameter and spacing are key enablers for high wetting breakthrough pressure and robustness.

Mechanical robustness. The key mechanical failures for the pillar array surface are pillar bending and buckling. Figure 9 shows the mechanical model we use to assess the mechanical properties of the pillar array surface.

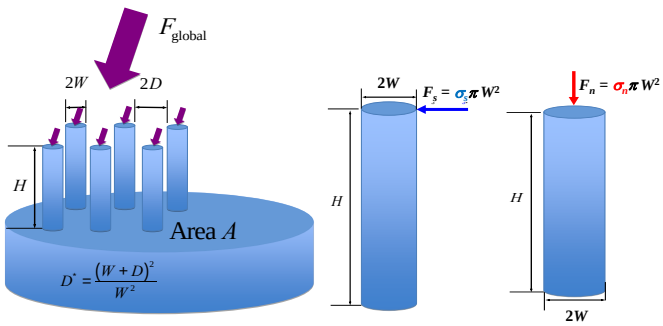

Fig. 9 Model pillar array surface used to model the deformation against external force F_{global}.

When an arbitrary force F_{global} is applied to the pillar array surface, it can decompose into a shear force (F_s) and a normal force (F_n), which may lead to bending and buckling failure if the force exceeds the mechanical limits of the structure and/or material. According to the classic Solid Mechanics theory of a circular shape beam with one fixed end and one free end, the dimensionless bending parameter S* and buckling parameter N* can be derived as follows [5].

$$S^* = \frac{\pi}{16}\left(\frac{E\gamma}{r_0}\right)^{\frac{1}{2}}\left(\frac{F_{s,global}}{A}\right)^{-1}(D^*)^{-1}\left(\frac{H}{W}\right)^{-1} \quad \text{Eq(1)}$$

$$N^* = \frac{\pi^3 E}{64}\left(\frac{F_{n,global}}{A}\right)^{-1}(D^*)^{-1}\left(\frac{H}{W}\right)^{-2} \quad \text{Eq(2)}$$

where E is Young's modulus of the material composing the pillar, γ is surface energy of the material, and r_0 is the distance between neighboring atoms.

When S^* and N^* are at 1.0, the critical stresses leading to mechanical failure can be calculated. Intuitively, pillar array surface with a high aspect ratio (large H/W) is expected to be weak mechanically. To balance wetting and mechanical properties, the minimum height for the pillar would be the one just tall enough to avoid wetting the bottom of the array surface due to liquid droplet sagging between pillars. For the 12 μm pitch pillar array surface, the critical height (H_c) is ~1 μm according to results in Figures 5 and 6. As the pitch is decreased, H_c will decrease as well. Assuming a superoleophobic surface is constructed with $H > H_c$, the overall wetting results and Eq (1) and (2) suggest that the other key design parameters for surface properties and robustness in mechanical properties and wetting breakthrough pressure are D* and pillar diameter.

4 SUMMARY AND REMARKS

In summary, we show in this work that both pillar size and spacing have relatively little effect on the super (water and oil) repellency where the static and advancing contact angles of the pillar array FOTS surfaces remain unchanged at ~150° and ~160° for water and hexadecane, respectively. On the other hand, sliding angle, receding angle and hysteresis are all found to be sensitive to surface texturing. Specifically, the receding angle is shown to decrease and sliding angle and hysteresis increase as the solid area fraction increases. The surface texturing effect is stronger for hexadecane as compared to water. The overall effect can be attributed to where the contact line is pinned in the pillar structure. For instance, while droplet of hexadecane is shown to pin underneath the re-entrant structure, water on the other hand pins on the pillar surface. Since de-pinning the contact line is the first step for drop receding and sliding [7-9], the surface texturing effect on the receding angle and hysteresis is rational.

Surface Evolver modeling is applied to understand the effect of surface texturing on the robustness of the liquid drop against external wetting breakthrough pressure. Our results show that the key design parameters for high breakthrough pressure are the phobicity of the surface, pillar diameter and spacing. Breakthrough pressure against wetting increases as the contact angle increases and as pillar size & spacing decrease. Mechanical modeling suggests that the key design parameters for high mechanical property are the low aspect ratio (H/W) and low D* value. While large diameter pillar will enhance mechanical robustness, it will adversely reduce the wetting breakthrough pressure. Depending on the design target or application, tradeoff between mechanical and wetting may be required.

5 ACKNOWLEDGEMENTS

The authors thank the staff at the Cornell Nanoscale Facility for the technical support of this work.

REFERENCES

[1] W. Barthlott and C. Neinhuis, Planta, 202, 1, 1997; also C. Neinhuis and W Barthlott, Annals. Botany, 79, 667, 1997.
[2] A. Tuteja, W. Choi, G. H. McKinley, R. E. Cohen and M. F. Rubner, MRS Bulletin, 33, 752, 2008.
[3] H. Zhao, K. Y. Law and V. Sambhy, Langmuir, 27, 5927, 2011.
[4] K. A. Brakke, The Surface Evolver. Experimental Mathematics, 1(2), 141, 1992.
[5] L.S. Srinath, Advanced Mechanics of Solids, 3rd ed.; Tata McGraw-Hill Education, 2009.
[6] H. Zhao, K-C Park and K. Y. Law, manuscript in preparation.
[7] J. W. Krumpfer, P. Bian, P Zhang, L. Gao and T. J. McCarthy, Langmuir, 27, 2166, 2011.
[8] C. Lv, C. Yang, P. Hao, F. He and Q. Zhang, Langmuir, 26, 8704, 2010.
[9] C. Dorrer and J. Ruhe, Langmuir, 22, 7657, 2006.